catalysts

MDPI

Article

In Situ Formation of Z-Scheme Bi_2WO_6/WO_3 Heterojunctions for Gas-Phase CO_2 Photoreduction with H_2O by Photohydrothermal Treatment

Zekai Zhang *, Ding Zhang, Lin Lyu, Guokai Cui and Hanfeng Lu *

Department of Industry Catalysis, College of Chemical Engineering, Zhejiang University of Technology, Chaowang Road 18, Hangzhou 310014, China
* Correspondence: zzk@zjut.edu.cn (Z.Z.); luhf@zjut.edu.cn (H.L.)

Abstract: We report a new photohydrothermal method to prepare a Bi_2WO_6/WO_3 catalytic material for CO_2 photoreduction by solar concentrators. The photohydrothermal treatment improves the physico-chemical properties of the Bi_2WO_6/WO_3 material and forms well contact Bi_2WO_6/WO_3 heterojunctions, which increase the maximum reaction rate of CO_2 photoreduction to 8.2 times under the simulated light, and the hydrocarbon yield under the real concentrating solar light achieves thousands of $\mu mol \cdot g_{cata}{}^{-1}$. The reason for the high activity is attributed to the direct Z-scheme effect of Bi_2WO_6/WO_3 heterojunctions and the photothermal effect during the course. These findings highlight the utilization of solar energy in CO_2 photoreduction and open avenues for the rational design of highly efficient photocatalysts.

Keywords: CO_2 photoreduction; photohydrothermal treatment; heterojunctions; solar energy

Citation: Zhang, Z.; Zhang, D.; Lyu, L.; Cui, G.; Lu, H. In Situ Formation of Z-Scheme Bi_2WO_6/WO_3 Heterojunctions for Gas-Phase CO_2 Photoreduction with H_2O by Photohydrothermal Treatment. *Catalysts* **2022**, *12*, 1237. https://doi.org/10.3390/catal12101237

Academic Editor: Kuan Chang

Received: 5 September 2022
Accepted: 12 October 2022
Published: 14 October 2022

1. Introduction

Solar energy is a massive, free, and non-polluting renewable energy source. Increasing the utilization efficiency of solar energy is one of the best solutions for a sustainable society. To facilitate storage and terminal utilization, it is better to convert solar energy into other forms, such as electricity or chemical compounds [1–3]. Photocatalytic reduction of CO_2 with H_2O, as occurs in green plants, can generate platform compounds with abundant energy such as CH_4 and methanol, and thus forms one of the main routes for solar energy transformation [4–6].

CO_2 photoreduction depends on the energy input of solar light and the function of the photocatalyst. CO_2 photoreduction entails the adsorption of photons in the incident light to generate electron-hole pairs, the separation/migration of photon-generated charge carriers, and the surface reaction of charge carriers with reactants [7–9]. Therefore, a desirable photocatalyst has high light harvesting efficiency, charge separation efficiency, charge migration and transport efficiency, and charge utilization efficiency for photocatalysis, and the promotion of any step is beneficial for the general efficiency. Tremendous efforts have been devoted to the development of effective photocatalysts [10]. However, at present, the general solar energy conversion efficiency remains at a poor level. This is because CO_2 molecules are stable, which means that only a small part of shortwave high-energy photoelectrons in solar light can activate them. Secondly, there are many reaction steps from CO_2 to hydrocarbon, while the recombination of the photo-generated electron-hole pair only needs one step, which is unfavorable to CO_2 reduction [11,12]. Most solar energy is thus converted into useless low-grade heat, which severely hinders the progress of CO_2 photoreduction.

The recombination of the photo-generated electron-hole pair also threatens the process intensification of CO_2 photoreduction, as the higher the incident light intensity, the more recombination of the pairs. Therefore, only few researchers have conducted studies in

this domain. Rossetti et al. [13] proposed a concept of a high-pressure photoreactor that can operate under pressure up to 20 bar. Wu et al. [14] increased some incident light of a fiber reactor with a spherical solar concentrator. With an additional step, solar energy can generate high-grade heat by large solar concentrators. The high-grade heat then can couple with the light to yield a photothermal approach, i.e., a catalytic process driven by the photochemical and thermochemical forces together [15].

The photothermal approach also broadens the absorption of the solar spectrum and provides a competitive way of raising the efficiency of solar energy transformation. The high incident light intensity by concentrating technology will contribute to a considerable increase in the CO_2 reaction rate. With the same catalyst, the CO_2 reaction rate under concentrating conditions can reach hundreds of times the rate under non-concentrating situations [16,17].

More interestingly, the photothermal effect is extended to the catalytic materials' preparation process. It is known that high-temperature hydrothermal treatment is a useful method to improve the properties of different materials, such as TiO_2 nanotubes, zeolites, etc. [18,19]. The high temperature and pressure can change the physical properties of the crystallized anatase powder, in turn improving the subsequent phase change properties of the anatase/rutile phase change. Similarly, photohydrothermal treatment, i.e., an environment with high light intensity, temperature, and pressure conditions, is expected to evolve the catalytic materials into a new, profitable state.

Bi_2WO_6 (band gap 2.8 eV) is one of the most studied catalysts in CO_2 photoreduction [20–26]. It has been demonstrated to be an active photocatalyst in the visible light band, and the formation of heterojunctions of Bi_2WO_6 with some other oxides, such as TiO_2 or WO_3, can further improve the activity [27,28]. However, it is necessary to find a new way to realize the well contact of two oxide phases and obtain adequate heterojunctions. In this manuscript, we present a new photohydrothermal method to promote the formation of Bi_2WO_6/WO_3 material with heterojunctions. The CO_2 photoreduction tests show that the Bi_2WO_6/WO_3 catalyst has favorable photocatalytic activity under simulated and real solar light. Furthermore, we propose the possible mechanism of CO_2 photoreduction in the reaction process. The photohydrothermal route can be a novel green technology for the preparation of similar materials and broaden the solar energy utilization scope.

2. Results and Discussions

2.1. CO_2 Photoreduction Performance of Bi_2WO_6/WO_3 under Real and Simulated Light

Figure 1 displays the yield and distribution of CO_2 photoreduction products on photohydrothermally treated Bi_2WO_6/WO_3 materials driven by real solar light. At a concentration ratio (CR, the ratio of incident light area to the catalyst disc area) of 1, i.e., natural solar light without concentration, only CH_4 is detected, and the yield is about 2.57 $\mu mol \cdot g_{cata}^{-1} \cdot h^{-1}$ after 5 h of reaction. The yield is lower than that under simulated light from a 300 W Xe lamp, which is about 3.43 $\mu mol \cdot g_{cata}^{-1} \cdot h^{-1}$. Then, when the CR increases to 400, in addition to CH_4, two more products appear: C_2H_4 and C_2H_6. After 5 h, the average yield rate of CH_4 is about 166.13 $\mu mol \cdot g_{cata}^{-1} \cdot h^{-1}$, that of C_2H_4 is 56.42 $\mu mol \cdot g_{cata}^{-1} \cdot h^{-1}$, and that of C_2H_6 is 28.11 $\mu mol \cdot g_{cata}^{-1} \cdot h^{-1}$. The total CO_2 conversion reaches 125.33 μmol and 1.12% in the reactor. The average rate increases to CH_4 304.94 $\mu mol \cdot g_{cata}^{-1} \cdot h^{-1}$, C_2H_4 62.70 $\mu mol \cdot g_{cata}^{-1} \cdot h^{-1}$, and C_2H_6 54.66 $\mu mol \cdot g_{cata}^{-1} \cdot h^{-1}$, and the total CO_2 conversion reaches 211.15 μmol and 1.89% (Tables 1 and 2) at CR 600. However, all the yield rates decrease when the CR continually increases to 800.

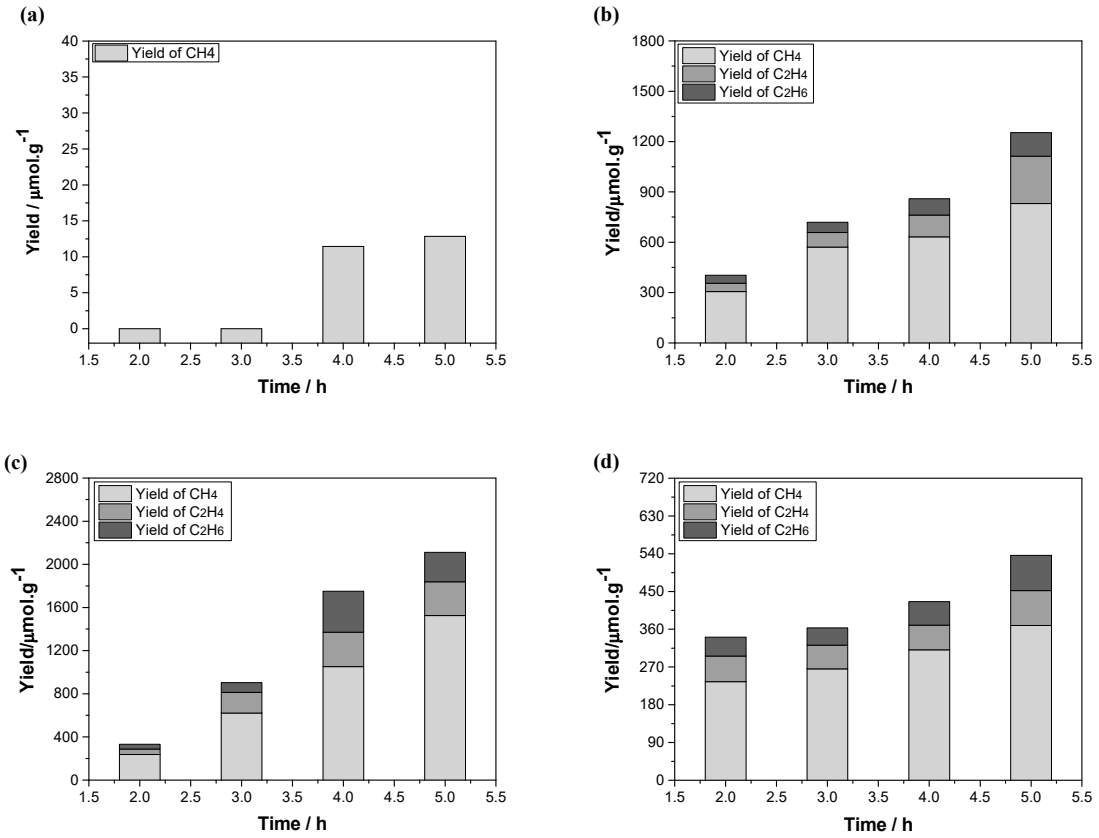

Figure 1. CO_2 photoreduction behavior of Bi_2WO_6/WO_3 under different concentration ratios (CRs): (**a**) natural light (CR = 1, 60 °C); (**b**) natural light (CR = 400, 300 °C); (**c**) natural light (CR = 600, 400 °C); (**d**) natural light (CR = 800, 500 °C).

Table 1. STC average efficiencies of Bi_2WO_6/WO_3 under concentrating solar light.

CR	Yield/μmol·g^{-1}			$STC_{average}$/%		CO_2 Conversion/%
	CH_4	C_2H_4	C_2H_6	UV	Total	
400	830.67	282.09	140.54	0.42	0.03	1.12
600	1524.70	313.52	273.31	0.72	0.05	1.89
800	368.95	83.05	84.05	0.28	0.02	0.63

The STC is calculated based on the total incident light intensity in Hangzhou, 58 mW/cm^2, and the UV part is considered to be 7% of the total light.

Table 2. STC max efficiencies of Bi_2WO_6/WO_3 under concentrating solar light.

CR	Yield/μmol·g^{-1}			STC_{max}/%	
	CH_4	C_2H_4	C_2H_6	UV	Total
400	198.31	152.42	43.33	0.84	0.06
600	430.18	127.79	288.29	1.73	0.12
800	117.50	30.42	22.73	0.28	0.02

The transformation efficiency of solar energy to chemical (STC) is calculated according to the formula:

$$STC = \frac{\text{Output energy as a chemical}}{\text{Energy of incident solar light}} = \frac{r \times \Delta G_r}{P_{sun} \times S} \quad (1)$$

where r is the product yield rate, ΔG_r is the Gibbs free energy, and P_{sun} and S are the incident light intensity and incident light area, respectively. From Tables 1 and 2, it can be seen that the maximum STC can reach 0.12% in the total solar light spectrum.

A large concentration ratio can raise the reaction temperature, which will give the impression that the high reaction rate is from the reaction conditions and not from the catalyst properties. Therefore, the yield and distribution of CO_2 photoreduction products on the Bi_2WO_6/WO_3 catalysts treated by the photohydrothermal method with different times were tested using a simulated light (a 300 W Xe lamp) reactor system, as shown in Figure 2. On Bi_2WO_6/WO_3 without photohydrothermal treatment, only CH_4 is detected, and the yield is about 17.14 $\mu mol \cdot g_{cata}^{-1}$ after 5 h of reaction. The yield is slightly larger than that under the natural light in Figure 1. Then, when it is photohydrothermally treated at CR 600 for 3 h, C_2H_4 appears. After a 3 h reaction, the yield of CH_4 reaches 101.44 $\mu mol \cdot g_{cata}^{-1}$ and that of C_2H_4 reaches 27.10 $\mu mol \cdot g_{cata}^{-1}$. The total CO_2 conversion reaches 128.54 $\mu mol \cdot g_{cata}^{-1}$. When the photohydrothermal treatment time prolongs to 5 h, both C_2H_4 and C_2H_6 appear again. After a 5 h reaction, the yield of CH_4 reaches 143.38 $\mu mol \cdot g_{cata}^{-1}$. The total CO_2 conversion reaches 204.26 $\mu mol \cdot g_{cata}^{-1}$.

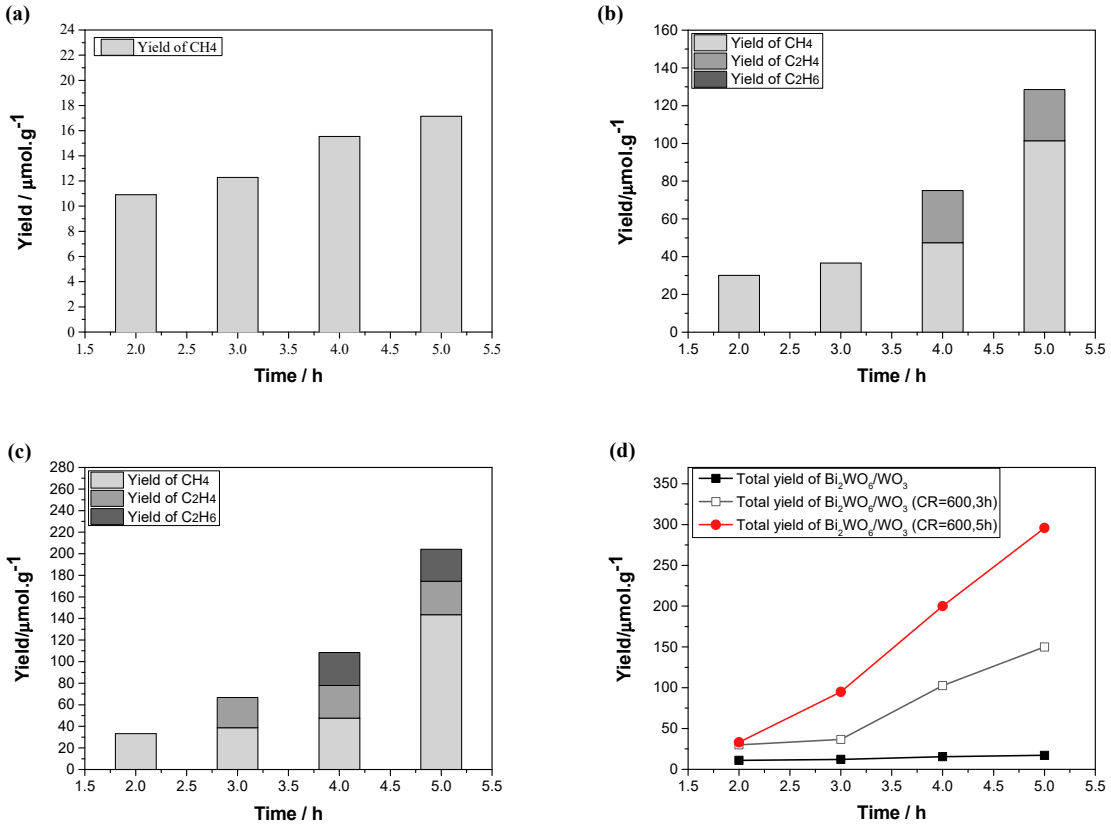

Figure 2. CO_2 photoreduction behavior of different Bi_2WO_6/WO_3 under a 300 W Xe lamp (CR = 8, 40 °C). (**a**) Bi_2WO_6/WO_3. (**b**) Bi_2WO_6/WO_3 treated for 5 h (natural light, CR = 600, 5 h). (**c**) Bi_2WO_6/WO_3 treated for 5 h (natural light, CR = 600, 5 h). (**d**) Total yield based on CO_2 conversion.

The results in Figures 1 and 2 illustrate that the catalytic activity of Bi_2WO_6/WO_3 material is improved after the photohydrothermal treatment. The appearance of ethylene and ethane also enriches the types of products, which means that it is possible to directly obtain C_2+ products by this route. The results are also reasonable, as the CO_2 photoreduction reaction is similar to the CO_2 hydrogenation reaction. In the reaction sequence of CO_2 reduction with H_2O, the H_2O first dissociates into H_2 and O_2, and then H_2 reacts with CO_2 [29]. The later reaction is known to be able to obtain molecules with multiple carbon atoms, such as ethanol, ethene, and even higher hydrocarbons [30]. High-carbon products are not often discussed, perhaps because the yield of these products is too low to be detected. Here, however, the high yield discloses their existence. The high yield proves that Bi_2WO_6/WO_3 is an excellent catalytic material for CO_2 photoreduction. The

results in Figure 1 also illustrate that Bi_2WO_6/WO_3 possesses high CO_2 photoreduction activity under real concentrating solar light. The CO_2 reaction rates at CR 400, 600, and 800 are several hundred times greater than the rate under natural light. It is known from the photocatalytic reaction kinetics that the order of light intensity in photocatalysis decreases with the incident light strength, i.e., the light utilization efficiency will decrease with the incident light strength, and the increment in incident light intensity cannot induce the corresponding increment in the reaction rate. Therefore, the CO_2 reaction rate here indicates that there might be another factor. The measured high temperatures in the reactor under high concentration ratios also indicate that the thermal effect is favorable for CO_2 photoreduction. In general, the CO_2 photoreduction results of Bi_2WO_6/WO_3 driven by the real and simulated solar light illustrate that there is a photothermal, even a photohydrothermal, effect yielded by the concentrating solar light technology, which is beneficial for the whole process.

2.2. Characterization of Bi_2WO_6 and Bi_2WO_6/WO_3 Samples

The texture properties of the Bi_2WO_6/WO_3 samples are listed in Table 3. The specific surface area of the sample does not change considerably after being treated at CR 400, while it noticeably decreases after being treated at CR 600 and 800. In addition, the average pore diameter increases with CR 600 and 800 treatment, which indicates the size growth in size of the nanoparticles.

Table 3. Texture properties of the Bi_2WO_6/WO_3 samples before and after photohydrothermal treatment.

Sample	Surface Area (m^2/g)	Pore Volume (cc/g)	Average Pore Diameter (nm)
Bi_2WO_6/WO_3	25.8	0.101	14.7
Bi_2WO_6/WO_3 (CR 400)	26.3	0.118	17.9
Bi_2WO_6/WO_3 (CR600)	17.0	0.217	51.2
Bi_2WO_6/WO_3 (CR800)	5.6	0.119	85.2

The crystal structures of the pure Bi_2WO_6 and Bi_2WO_6/WO_3 samples were detected by XRD technology. The results are shown in Figure 3. The characteristic peaks of Russellite Bi_2WO_6 (JCPDS no. 26-1044) and the monoclinic WO_3 (JCPDS no. 43-1035) can be identified by the patterns. After photohydrothermal treatment, the diffraction peaks of the samples changed. As seen in Figure 3, the peaks of WO_3 at values of 23.2°, 23.6°, and 24.4° corresponding to (002), (020), and (200) shift slightly and transform into two diffraction peaks corresponding to (020) and (200). [31] The feature peaks of Bi_2WO_6 at values of 28.6° and 33.03° become clearer.

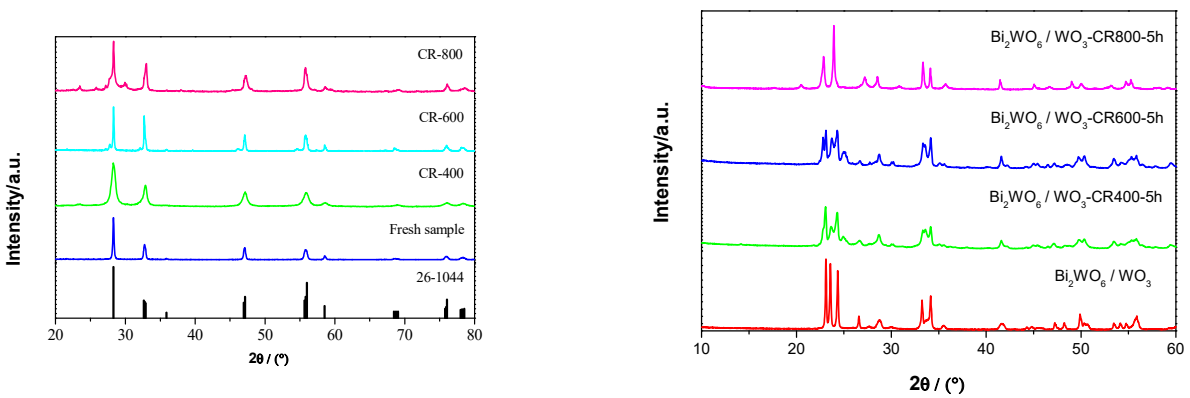

Figure 3. XRD patterns of parent and photohydrothermally treated Bi_2WO_6 and Bi_2WO_6/WO_3 under different concentration ratios: (**left**) Bi_2WO_6; (**right**) Bi_2WO_6/WO_3.

The morphology and microstructure of Bi_2WO_6/WO_3 before and after photohydrothermal treatment were investigated using SEM and TEM. Typical cuboids with a moderate size were found in the parent Bi_2WO_6/WO_3. The photohydrothermally treated Bi_2WO_6/WO_3 displays the size growth of the particles, which is also seen in TEM (Figure 4). From the TEM image of Bi_2WO_6/WO_3 heterojunction (Figure 5), the lattice fringes of the sample after photohydrothermal treatment are clearer than those of the parent sample. Two oxide phases of Bi_2WO_6 and WO_3 are more clearly observed and closely contact to form an intimate interface after photohydrothermal treatment. The value of 0.248 nm corresponds to the (202) crystallographic plane of the orthorhombic Bi_2WO_6 crystal, which is also in accordance with the XRD results in Figure 3. The value of 0.342 nm corresponds to the (012) crystallographic plane of the WO_3. This result suggests that the photohydrothermal treatment could improve the Bi_2WO_6/WO_3 heterojunctions in the structure. The tight coupling is favorable for the charge transfer between WO_3 and Bi_2WO_6 and promotes the separation of photogenerated electron-hole pairs, subsequently improving the photocatalytic activity.

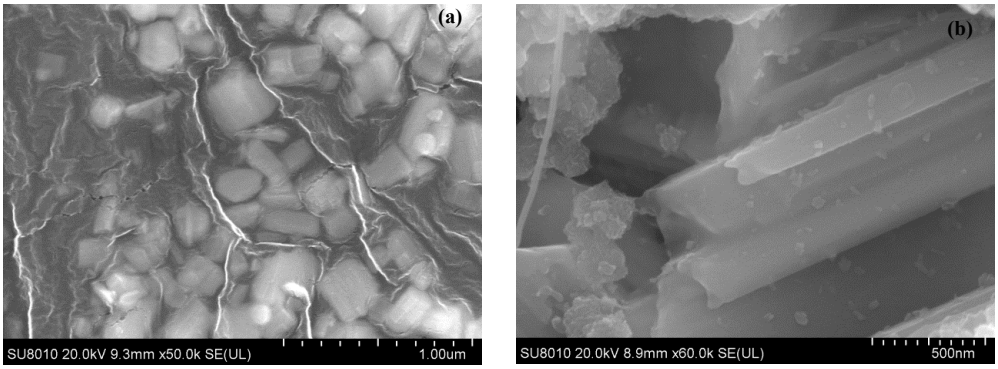

Figure 4. SEM images of (**a**) parent and (**b**) photohydrothermally treated Bi_2WO_6/WO_3.

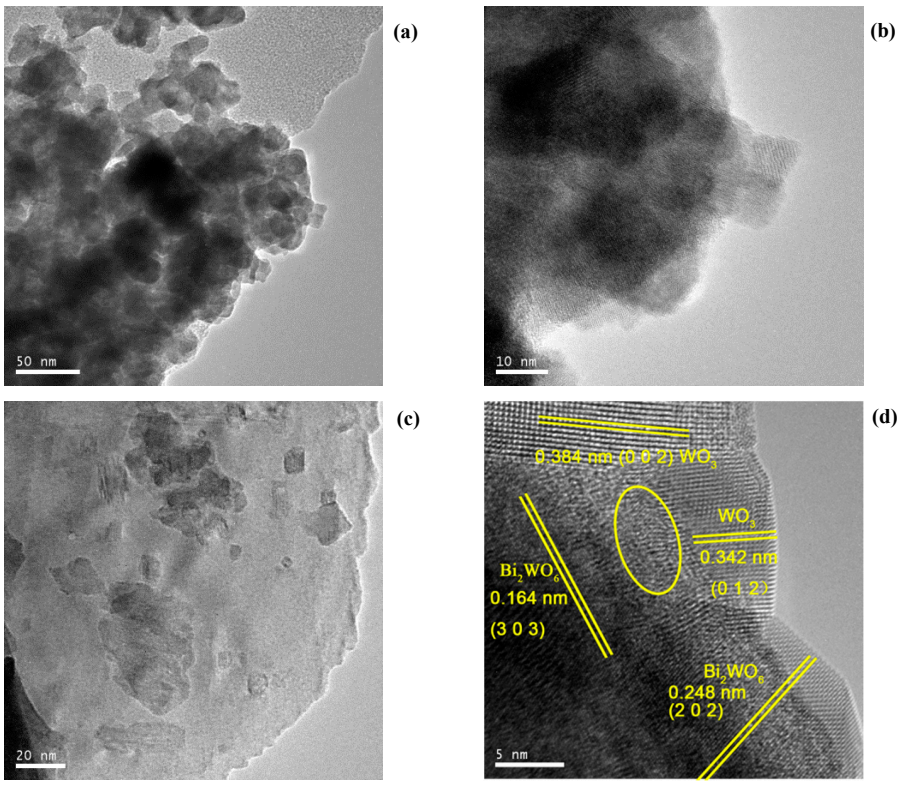

Figure 5. TEM images of (**a**,**b**) parent and (**c**,**d**) photohydrothermally treated Bi_2WO_6/WO_3 (natural light, CR = 600, 5 h).

The composition and valance state of Bi_2WO_6/WO_3 are demonstrated via XPS technology, and the spectra are shown in Figure 6. The XPS spectra confirm that Bi, W, and O elements coexist in the samples. Figure 6a shows that the typical peak of O 1s, located at around 530 eV, can be deconvoluted into two peaks from the lattice Bi–O and W–O. After photohydrothermal treatment, a new peak appears from O–H or oxygen vacancy. The characteristic peaks of W 4f (Figure 6) are located at 37.2 and 35.1 eV, which conform to W $4f_{5/2}$ and $4f_{7/2}$, respectively, revealing that W presents with W^{6+}. Figure 6c shows that two peaks at 164.2 and 158.9 eV exist on the XPS spectrum of Bi, which are related to Bi $4f_{5/2}$ and Bi $4f_{7/2}$, respectively. The phenomenon demonstrates that Bi exists in the photocatalyst with Bi^{3+} [32,33]. After the treatment, the two peaks slightly move toward a lower altitude, indicating the interaction between Bi_2WO_6 and WO_3.

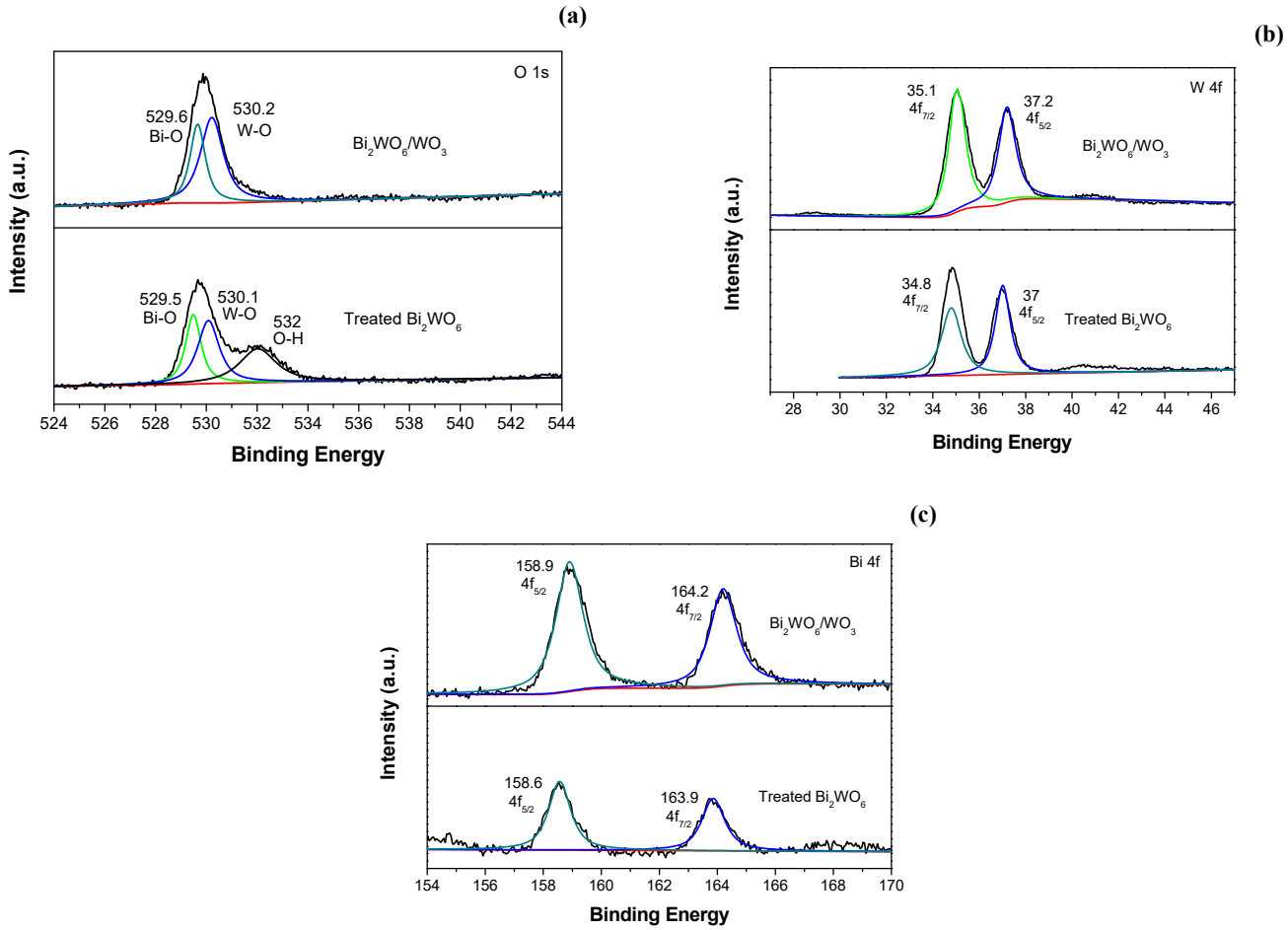

Figure 6. XPS spectra of parent and photohydrothermally treated Bi_2WO_6/WO_3 (natural light, CR = 600, 5 h): (**a**) O 1s; (**b**) W 4f; (**c**) Bi 4f.

2.3. Discussions

The catalytic performance of Bi_2WO_6/WO_3 under real and simulated solar light proves two points:

1. The photohydrothermal treatment improves the catalytic performance of Bi_2WO_6/WO_3 under real light and 300 W Xe light.

2. The catalytic performance of Bi_2WO_6/WO_3 under simulated solar light from a 300 W Xe source further confirms that the effect is part of the improvement in catalyst properties, as the reaction conditions provided by Xe light are similar to the classic CO_2 photoreduction reaction conditions, which exclude the possible influence from the reaction conditions provided by real concentrating solar light.

We then analyzed how the photohydrothermal treatment influences Bi_2WO_6/WO_3. By the characterizations, it can be seen that the photohydrothermal treatment decreases the specific surface area (BET), decreases the crystallinity of Bi_2WO_6 or WO_3 (XRD), and increases the particle sizes (SEM). All of these changes do not appear beneficial for the catalytic activity. Considering the characterization and our initial intention, it is reasonable to accept that the formation of the Bi_2WO_6/WO_3 heterojunctions (TEM and XPS) is a possible reason for such activity. To increase the likelihood of the hypothesis, the activity of the pure Bi_2WO_6 and WO_3 with real light as the source was tested, as shown in Figure 7 and Figure S2. It can be seen that pure Bi_2WO_6 and WO_3 are lower than Bi_2WO_6/WO_3 under the same conditions.

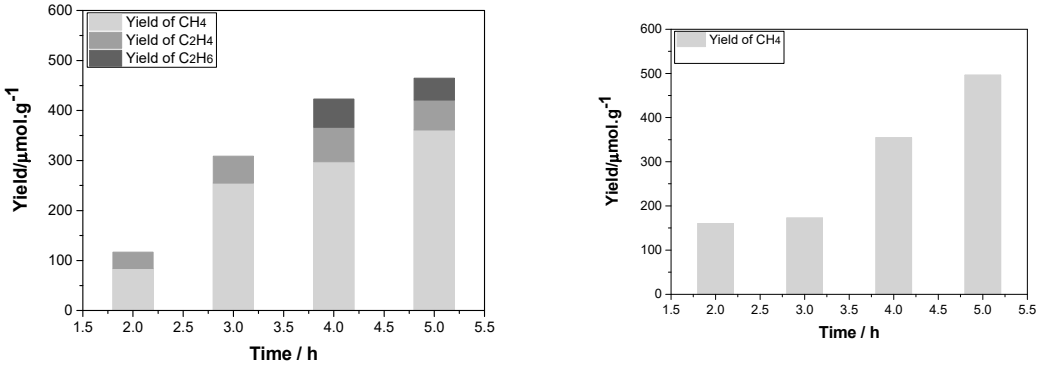

Figure 7. CO_2 photoreduction behavior of pure Bi_2WO_6 (**left**) and WO_3 (**right**) (natural light, CR = 600).

In general, the activity promotion of Bi_2WO_6/WO_3 does not stem from the specific surface area, as the specific surface area decreases. It also does not come from the crystallinity, as can be seen in Figure 3. The activity of the pure Bi_2WO_6 and WO_3 material with the same preparation procedure is proven to be lower than that of the Bi_2WO_6/WO_3 materials. That is to say, the interaction of Bi_2WO_6/WO_3 must have happened in some respect, and this is favorable for CO_2 photoreduction. The interaction between two species is often called the support effect in thermal catalysis, while in the photocatalyst field, it is often called a heterojunction. Although more evidence is needed, it appears reasonable to adopt the heterojunction theory to explain the results here [34,35].

In Bi_2WO_6-related materials, it is common to construct a heterojunction structure by adjusting the components of Bi or W elements. For example, Aranda-Aguirre et al. [36] prepared Bi_2O_3/Bi_2WO_6 thin films for the photo-electrocatalytic degradation of histamine. Chung et al. [37] constructed Bi_2WO_6 and WO_3 heterojunction photoanodes for improved charge transportation, and He et al. [38] synthesized a core/shell WO_3 (core)/Bi_2WO_6 (shell) structure. Gui et al. [39] achieved the heterojunction of Bi_2WO_6/WO_3 with a one-step hydrothermal method in 2012. In 2020, Chen et al. [40] further discussed the Bi_2WO_6/WO_3 heterojunction by facet engineering with salicylic acid removal reaction. Under visible light irradiation, Bi_2WO_6 and WO_3 are excited simultaneously, and electron-hole pairs are generated. For certain faces, i.e., WO_3(001) and (110)/Bi_2WO_6, the photogenerated electrons can instantly transfer from CB of WO_3 to VB of Bi_2WO_6, and then combine with the holes of Bi_2WO_6, leading to the high-efficiency carriers' separation in the composite.

Based on the results and discussion above, a possible direct Z-scheme photocatalytic mechanism for the Bi_2WO_6/WO_3 heterojunctions in CO_2 photoreduction is proposed and schematically exhibited in Scheme 1. Under the incident light irradiation, both Bi_2WO_6 and WO_3 could be excited to generate electrons (e^-) and holes (h^+). Then, the photogenerated electrons of WO_3 will transfer to the valence band of Bi_2WO_6, leaving the electrons in Bi_2WO_6 and the holes in WO_3, resulting in electrons with higher reduction potential in Bi_2WO_6 and holes with higher oxidation potential in WO_3. The electrons in Bi_2WO_6 will react with the adsorbed CO_2 and reduce it to hydrocarbons. The accumulated holes in WO_3 will be consumed by oxidizing H_2O to O_2. Therefore, the Bi_2WO_6/WO_3 heterojunctions

form a direct Z-scheme structure and show the efficient activity of photocatalytic CO_2 reduction and selectivity toward hydrocarbons.

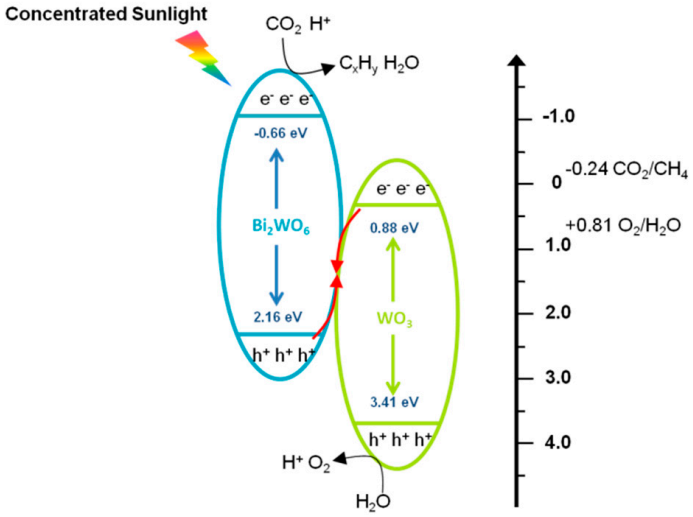

Scheme 1. Schematic diagram of CO_2 photoreduction with H_2O in Bi_2WO_6/WO_3.

Finally, we investigated if the effect of photohydrothermal treatment is better than the effect of the normal hydrothermal treatment. We tested the activity of Bi_2WO_6/WO_3 treated by the normal hydrothermal method, as shown in Figure 8. The activity of the normal hydrothermal method is lower than that of the photohydrothermal method. The light must play a role and induce the crystal growth. Thus, photohydrothermal treatment has certain merits.

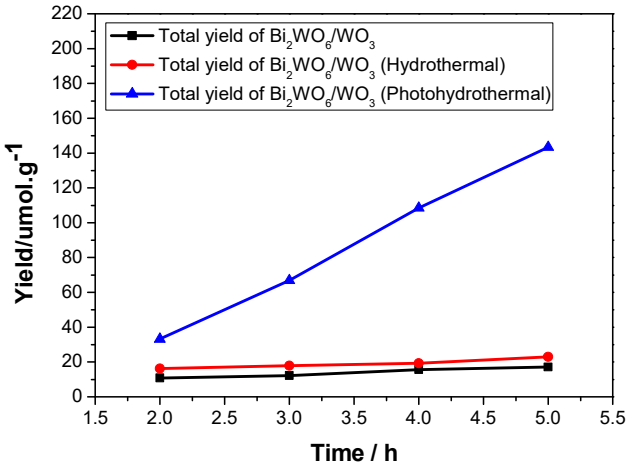

Figure 8. CO_2 photoreduction behavior of different Bi_2WO_6/WO_3 under a 300 W Xe lamp (CR = 8, 40 °C): black line—Bi_2WO_6/WO_3; red line—Hydrothermal treated WO_6/WO_3 (400 °C, 5 h); blue line—Photohydrothermally treated Bi_2WO_6/WO_3 (natural light, CR = 600, 5 h).

3. Materials and Methods

The pure Bi_2WO_6 and parent Bi_2WO_6/WO_3 material were first prepared by a co-impregnation method. For the pure Bi_2WO_6, 0.9702 g of bismuth nitrate pentahydrate was dissolved in a 100 mL beaker with 20 mL of deionized water under stirring. When white precipitation appeared, the pH was adjusted until the white precipitation disappeared, and 2 g of sodium dodecyl sulfate surfactant was added to obtain solution A. To obtain solution B, 0.254 g of hydrate ammonium tungstate was added to another 100 mL beaker with 20 mL of water in a water bath at 80 °C under stirring. Solution B was then added to

solution A dropwise with stirring to yield solution C. Then, 5 mL of ethylene glycol was added to solution C and its pH was adjusted to 7. After stirring solution C for 2 h, it was transferred to a clean autoclave and placed in an oven at 160 °C for 20 h. The sample was taken out and washed several times with deionized water and ethanol, dried in an 80 °C oven overnight, and finally calcined in a muffle at 500 °C for 2 h.

For the parent Bi_2WO_6/WO_3, excess 0.4 g WO_3 powder was added to solution A during the solution's preparation step [41,42]. The photohydrothermal treatment of the Bi_2WO_6/WO_3 sample was carried out in a homemade concentrating solar reactor system. A detailed illustration of the system can be seen in the Supplementary Materials. A proper amount of the Bi_2WO_6/WO_3 sample was put into the reactor with a certain amount of liquid H_2O. The reactor was then sealed and purged with highly pure CO_2 gas for 30 min to remove the impure gases from the reactor. The reactor was fixed on the concentrating solar light system. By the detector and meter, the reactor angle was adjusted to let solar light enter the reactor to reach a certain light intensity, temperature, and pressure. The treatment was maintained for certain time (1–2 h).

The crystal structures of the pure Bi_2WO_6 and Bi_2WO_6/WO_3 materials before and after reaction were characterized by an X-ray diffractometer apparatus with Cu-Kα source (X'Pert PRO, PNAlytical, The Netherlands). The scanning angle was set from 10° to 80° (2θ) with a rate of 0.02°. The surface morphology picture of the Bi_2WO_6/WO_3 material was taken by an FESEM apparatus (field emission scanning electron microscopy, Hitachi S-4700, Hitachi Ltd., Chiyoda, Japan). The voltage range was 0.5–30 kV, and the acceleration voltage was set to 15 kV. The HRTEM (Tecnai G2 F30 S-Twin, FEI, The Netherlands) was used to distinguish the morphology change in the Bi_2WO_6/WO_3 materials before and after the reaction. The valence state of the Bi_2WO_6/WO_3 material was recorded by XPS spectra on a clutches spectrophotometer(Kratos AXIS Ultra DLD, Shimadzu, Kyoto, Japan).

Experiments of the photocatalytic reduction of CO_2 reactivity were performed under a 300 W Xe lamp and natural light. Before the reaction began, the reactor was cleaned and dried. Deionized water was added, and CO_2 gas was used to check for leakage, remove impure gases, and act as a reactant. Sampling analysis was performed every 1 h. The light intensity was measured with a light intensity meter, and the temperature was recorded by a k-type thermocouple. Samples were analyzed by gas chromatography (GC-2014, Shimadzu, Kyoto, Japan) with an FID detector equipped with HT-PLOT Q capillary columns that can detect various hydrocarbon compounds from C1 to C6.

4. Conclusions

We report a new photohydrothermal method for photocatalyst preparation. The photohydrothermal treatment can reconstruct the morphology of the Bi_2WO_6/WO_3 material and form well contact Bi_2WO_6/WO_3 heterojunctions, showing high CO_2 photoreduction activity under the simulated and concentrating real solar light. The photothermal and photohydrothermal effects are expected to be beneficial not only for the CO_2 photoreduction reaction but also for the preparation of similar photocatalysts, and accelerate the research progress of solar fuels.

Supplementary Materials: The following are available online at https://www.mdpi.com/xxx/s1, Figure S1: Homemade high concentrating light reactor system, Figure S2. CO_2 photoreduction behavior of pure WO_3, Figure S3. XRD pattern of pure Bi_2WO_6.

Author Contributions: Conceptualization, Z.Z. and H.L.; methodology, L.L. and D.Z.; writing—original draft preparation, L.L. and D.Z.; writing—review and editing, Z.Z. and G.C.; funding acquisition, H.L. and G.C. All authors have read and agreed to the published version of the manuscript.

Funding: Natural Science Foundation of China as general projects (grant no. 21506194, 21676255).

Data Availability Statement: The data will be available at request.

Conflicts of Interest: The authors declare no conflict of interest.

References

1. Shih, C.F.; Zhang, T.; Li, J.; Bai, C. Powering the Future with Liquid Sunshine. *Joule* **2018**, *2*, 1925–1949. [CrossRef]
2. Weinstein, L.A.; Loomis, J.; Bhatia, B.; Bierman, D.M.; Wang, E.N.; Chen, G. Concentrating Solar Power. *Chem. Rev.* **2015**, *115*, 12797–12838. [CrossRef] [PubMed]
3. Devens, G.; Moore, T.A.; Moore, A.L. Solar fuels via artificial photosynthesis. *Acc. Chem. Res.* **2009**, *42*, 1890–1898.
4. He, J.; Janáky, C. Recent Advances in Solar-Driven Carbon Dioxide Conversion: Expectations versus Reality. *ACS Energy Lett.* **2020**, *5*, 1996–2014. [CrossRef]
5. Ulmer, U.; Dingle, T.; Duchesne, P.N.; Morris, R.H.; Tavasoli, A.; Wood, T.; Ozin, G.A. Fundamentals and applications of photocatalytic CO_2 methanation. *Nat. Commun.* **2019**, *10*, 3169–3181. [CrossRef]
6. Roy, S.C.; Varghese, O.K.; Paulose, M.; Grimes, C.A. Toward Solar Fuels: Photocatalytic Conversion of Carbon Dioxide to Hydrocarbons. *ACS Nano* **2010**, *4*, 1259–1278. [CrossRef]
7. Jiao, X.; Zheng, K.; Liang, L.; Li, X.; Sun, Y.; Xie, Y. Fundamentals and challenges of ultrathin 2D photocatalysts in boosting CO_2 photoreduction. *Chem. Soc. Rev.* **2020**, *49*, 6592–6604. [CrossRef]
8. Nguyen, V.-H.; Wu, J.C. Recent developments in the design of photoreactors for solar energy conversion from water splitting and CO_2 reduction. *Appl. Catal. A* **2018**, *550*, 122–141. [CrossRef]
9. Li, X.; Yu, J.; Jaroniec, M.; Chen, X. Cocatalysts for Selective Photoreduction of CO_2 into Solar Fuels. *Chem. Rev.* **2019**, *119*, 3962–4179. [CrossRef]
10. Habisreutinger, S.N.; Schmidt-Mende, L.; Stolarczyk, J.K. Photocatalytic Reduction of CO_2 on TiO_2 and Other Semiconductors. *Angew. Chem. Int. Ed.* **2013**, *52*, 7372–7408. [CrossRef]
11. Teramura, K.; Tanaka, T. Necessary and sufficient conditions for the successful three-phase photocatalytic reduction of CO_2 by H_2O over heterogeneous photocatalysts. *Phys. Chem. Chem. Phys.* **2018**, *20*, 8423–8437. [CrossRef]
12. Kondratenko, E.V.; Mul, G.; Baltrusaitis, J.; Larrazábal, G.O.; Pérez-Ramírez, J. Status and perspectives of CO_2 conversion into fuels and chemicals by catalytic, photocatalytic and electrocatalytic processes. *Energy Environ. Sci.* **2013**, *6*, 3112–3135. [CrossRef]
13. Rossetti, I.; Villa, A.; Pirola, C.; Prati, L.; Ramis, G. A novel high-pressure photoreactor for CO_2 photoconversion to fuels. *RSC Adv.* **2014**, *4*, 28883–28885. [CrossRef]
14. Nguyen, T.-V.; Wu, J.C.; Chiou, C.-H. Photoreduction of CO_2 over Ruthenium dye-sensitized TiO_2-based catalysts under concentrated natural sunlight. *Catal. Commun.* **2008**, *9*, 2073–2076. [CrossRef]
15. Zhang, Z.; Wang, Y.; Cui, G.; Liu, H.; Abanades, S.; Lu, H. Improvement of CO_2 Photoreduction Efficiency by Process Intensification. *Catalysts* **2021**, *11*, 912. [CrossRef]
16. Ghoussoub, M.; Xia, M.; Duchesne, P.N.; Segal, D.; Ozin, G. Principles of photothermal gas-phase heterogeneous CO_2 catalysis. *Energy Environ. Sci.* **2019**, *12*, 1122–1142. [CrossRef]
17. Shi, L.; Wang, X.Z.; Hu, Y.W.; He, Y.R. Investigation of photocatalytic activity through photo-thermal heating enabled by Fe_3O_4/TiO_2 composite under magnetic field. *Sol. Energy* **2020**, *196*, 505–512. [CrossRef]
18. Wong, C.L.; Tan, Y.N.; Mohamed, A.R. A review on the formation of titania nanotube photocatalysts by hydrothermal, treatment. *J. Environ. Manag.* **2011**, *92*, 1669–1680. [CrossRef]
19. Dusselier, M.; Deimund, M.A.; Schmidt, J.E.; Davis, M.E. Methanol-to-Olefins Catalysis with Hydrothermally Treated Zeolite SSZ-39. *ACS Catal.* **2015**, *5*, 6078–6085. [CrossRef]
20. Liu, T.; Li, H.; Gao, J.; Ding, S.; Liu, X.; Jia, H.; Xue, J. Effect of oxygen vacancies on the photocatalytic CO2 reduction performance of Bi_2WO_6: DFT and experimental studies. *Appl. Surf. Sci.* **2021**, *579*, 152135. [CrossRef]
21. Yang, C.; Wang, Y.J.; Yu, J.G.; Cao, S.W. Ultrathin 2D/2D Graphdiyne/Bi2WO6 Heterojunction for Gas-Phase CO_2 Photoreuction. *ACS Appl. Energy Mater.* **2021**, *4*, 8734–8738. [CrossRef]
22. Liu, Y.; Shen, D.; Zhang, Q.; Lin, Y.; Peng, F. Enhanced photocatalytic CO_2 reduction in H_2O vapor by atomically thin Bi_2WO_6 nanosheets with hydrophobic and nonpolar surface. *Appl. Catal. B* **2020**, *283*, 119630. [CrossRef]
23. Ma, H.; He, Y.; Chen, P.; Wang, H.; Sun, Y.; Li, J.; Dong, F.; Xie, G.; Sheng, J. Ultrathin Two-Dimensional Bi-Based photocatalysts: Synthetic strategies, surface defects, and reaction mechanisms. *Chem. Eng. J.* **2021**, *417*, 129305. [CrossRef]
24. Xiong, J.; Di, J.; Li, H. Interface engineering in low-dimensional bismuth-based materials for photoreduction reactions. *J. Mater. Chem. A* **2020**, *9*, 2662–2677. [CrossRef]
25. Ribeiro, C.S.; Tan, J.Z.; Maroto-Valer, M.M.; Lansarin, M.A. Photocatalytic reduction of CO_2 over Bi_2WO_6 in a continuous-flow differential photoreactor: Investigation of operational parameters. *J. Environ. Chem. Eng.* **2021**, *9*, 105097. [CrossRef]
26. Ren, G.; Zhang, X.; Zhang, C.; Li, R.; Liu, J.; Wang, Y.; Wang, Y.; Fan, C.; Zhao, Q. Synergetic effect of Bi_2WO_6 micro-spheres and activated carbon mm-spheres for enhancing photoreduction activity of CO_2 to CO. *Mater. Lett.* **2019**, *264*, 127201. [CrossRef]
27. Xu, Q.C.; Wellia, D.V.; Ng, Y.H.; Amal, R.; Tan, T.T.Y. Synthesis of Porous and Visible-Light Absorbing Bi_2WO_6/TiO_2 Heterojunction Films with Improved Photoelectrochemical and Photocatalytic Performances. *J. Phys. Chem. C* **2011**, *115*, 7419–7428. [CrossRef]
28. Zhou, H.R.; Wen, Z.P.; Liu, J.; Ke, J.; Duan, X.G.; Wang, S.B. Z-scheme plasmonic Ag decorated WO_3/Bi_2WO_6 hybrids for enhanced photocatalytic abatement of chlorinated-VOCs under solar light irradiation. *Appl. Catal. B* **2019**, *242*, 76–84. [CrossRef]
29. Ma, Y.; Wang, X.; Jia, Y.; Chen, X.; Han, H.; Li, C. Titanium Dioxide-Based Nanomaterials for Photocatalytic Fuel Generations. *Chem. Rev.* **2014**, *114*, 9987–10043. [CrossRef]

30. Wang, L.X.; He, S.X.; Wang, L.; Lei, Y.; Meng, X.J.; Xiao, F.S. Cobalt–Nickel Catalysts for Selective Hydrogenation of Carbon Dioxide into Ethanol. *ACS Catal.* **2019**, *9*, 11335–11340. [CrossRef]
31. Huang, J.; Tan, G.Q.; Ren, H.J.; Yang, W.; Xu, C.; Zhao, C.C.; Xia, A. Photoelectric Activity of a $Bi_2O_3/Bi_2WO_{6-x}F_{2x}$ Heterojunction Prepared by a Simple One-Step Microwave Hydrothermal Method. *ACS Appl. Mater. Interfaces* **2014**, *6*, 21041–21050. [CrossRef]
32. Ng, C.; Iwase, A.; Ng, Y.H.; Amal, R. Transforming Anodized WO_3 Films into Visible-Light-Active Bi_2WO_6 Photoelectrodes by Hydrothermal Treatment. *J. Phys. Chem. Lett.* **2012**, *3*, 913–918. [CrossRef]
33. Mehta, N.; Kumar, A. Structural characterization of light-induced crystal growth in $Se_{98}Sb_2$ chalcogenide glass. *J. Non-Cryst. Solids* **2012**, *358*, 776–781. [CrossRef]
34. Low, J.; Jiang, C.; Cheng, B.; Swelm, W.; Al-Ghamdi, A.A.; Yu, J. A Review of Direct Z-Scheme Photocatalysts. *Small Methods* **2017**, *1*, 1700080. [CrossRef]
35. Zhang, Z.K.; Gao, Z.H.; Liu, H.Y.; Abanades, S.; Lu, H.F. High Photothermally Active Fe_2O_3 Film for CO_2 Photoreduction with H_2O Driven by Solar Light. *ACS Appl. Energy Mater.* **2019**, *2*, 8376–8380. [CrossRef]
36. Aranda-Aguirre, A.; de Oca, J.M.; Corzo, A.; Garcia-Segura, S.; Alarcon, H. Mixed metal oxide Bi_2O_3/Bi_2WO_6 thin films for the photoelectrocatalytic degradation of histamine. *J. Electronanaly. Chem.* **2022**, *919*, 116528. [CrossRef]
37. Chung, H.Y.; Wong, R.J.; Amal, R.; Ng, Y.H. Engineering the Interfacial Contact between Bi_2WO_6 and WO_3 Heterojunction Photoanode for Improved Charge Transportation. *Energy Fuels* **2022**, *36*, 11550–11558. [CrossRef]
38. He, G.H.; He, G.L.; Li, A.J.; Li, X.; Wang, X.J.; Fang, Y.P.; Xu, Y.H. Synthesis and visible light photocatalytic behavior of WO_3 (core)/ Bi_2WO_6 (shell). *J. Mole. Catal. A* **2014**, *385*, 106–111. [CrossRef]
39. Gui, M.S.; Zhang, W.D.; Chang, Y.Q.; Yu, Y.X. One-step hydrothermal preparation strategy for nanostructured WO_3/Bi_2WO_6 heterojunction with high visible light photocatalytic activity. *Chem. Eng. J.* **2012**, *197*, 283–288. [CrossRef]
40. Chen, X.; Li, Y.X.; Li, L. Facet-engineered surface and interface design of WO_3/ Bi_2WO_6 photocatalyst with direct Z-scheme heterojunction for efficient salicylic acid removal. *Appl. Sur. Sci.* **2020**, *508*, 144796. [CrossRef]
41. Tian, Y.L.; Chang, B.B.; Lu, J.L.; Fu, J.; Xi, F.N.; Dong, X.P. Hydrothermal Synthesis of Graphitic Carbon Nitride–Bi_2WO_6 Heterojunctions with Enhanced Visible Light Photocatalytic Activities. *ACS Appl. Mater. Interfaces* **2013**, *5*, 7079–7085. [CrossRef] [PubMed]
42. Ge, M.; Li, Y.F.; Liu, L.; Zhou, Z.; Chen, W. $Bi_2O_3-Bi_2WO_6$ Composite Microspheres: Hydrothermal Synthesis and Photocatalytic Performances. *J. Phys. Chem. C* **2011**, *115*, 5220–5225. [CrossRef]